Novel octahedral tilt system $a^+b^+c^+$ in (1-x)$Na_{0.5}Bi_{0.5}TiO_3$-$x$$CdTiO_3$ solid solutions

R. Ignatans, M. Dunce*, E. Birks, and A. Sternberg

Institute of Solid State Physics, University of Latvia, Kengaraga 8, Riga, LV-1063, Latvia
* Corresponding author. E-mail: marija.dunce@cfi.lu.lv. Tel.: +371 67260803. Fax: +371 67132778

Abstract

(1-x)$Na_{0.5}Bi_{0.5}TiO_3$-$x$$CdTiO_3$ solid solutions in the whole concentration range ($0.0 \leq x \leq 1.0$) were studied by means of x-ray diffraction, dielectric spectroscopy and polarization measurements. The study was mainly focused on crystalline structure of the compositions, depending on their place in the phase diagram. The solid solution system exhibits at least four different phases at room temperature, giving rise to paraelectric, ferroelectric and relaxor-ferroelectric behaviour. There were proposed appropriate space groups for each of these phases, using Rietveld refinement method for analysis of the x-ray diffraction patterns and taking into account polarization measurement results. Unexpected and unusual octahedral tilt systems – $a^+a^+a^+$ and $a^+b^+c^+$ – were found in certain $CdTiO_3$ concentration ranges. The tilt system $a^+b^+c^+$, which was detected in the ferroelectric phase, was evidenced for the first time, as it has been theoretically predicted, but never experimentally observed before in any material. It was shown that ferroelectricity in (1-x)$Na_{0.5}Bi_{0.5}TiO_3$-$x$$CdTiO_3$ solid solutions arises not only from the Ti^{+4} displacements, but also from the polar distortions in square planar and cubooctahedral cation A-sites. Upon heating, at a phase transition from the ferroelectric to the paraelectric state, $a^+b^+c^+$ tilt system transforms into $a^+a^+a^+$. The studied compositions were compared with (1-x)$Na_{0.5}Bi_{0.5}TiO_3$-$x$$CaTiO_3$ solid solution system, as $CdTiO_3$ and $CaTiO_3$ are crystallographically very similar. It was revealed that both constituents behave very differently. $CaTiO_3$ in (1-x)$Na_{0.5}Bi_{0.5}TiO_3$-$x$$CaTiO_3$, even in low concentrations, stabilizes solid solutions in its *Pnma* space group, unlike its counterpart $CdTiO_3$ in the studied materials.

KEYWORDS: structure, NBT, ferroelectrics, x-ray diffraction, tilt system, solid solution

Introduction

$Na_{0.5}Bi_{0.5}TiO_3$ (NBT) and its solid solutions have been actively studied recently as one of the most promising lead-free ferroelectric materials to possibly substitute the lead containing ferroelectric materials widely used in industry [1-3]. Although the ground state structure of pure NBT at room temperature is still under discussion, the crystal structure of the poled specimens undoubtedly has the space group *R3c* and the $a^-a^-a^-$ oxygen octahedral tilt system according to Glazer notation [4-6]. At elevated temperatures NBT has two additional distinct phases. Between 280˚C and ~510˚C NBT has tetragonal symmetry with the space group *P4bm* and above this temperature region it becomes cubic with the space group $Pm\bar{3}m$ [2,7]. Electron diffraction analysis of NBT in the temperature region above the depolarisation temperature (~200˚C) revealed superstructure maxima characteristic for the space group *Pnma* [8]. Recently coexistence of *R3c* and *Pnma* phases in non-poled NBT at room temperature was proposed [9].

$CdTiO_3$ undergoes an irreversible first-order phase transition near 900˚C from an ilmenite to a perovskite phase which allows it to be synthesized with either of the structures [10]. The room temperature perovskite phase is non-polar and isostructural with $CaTiO_3$ (space group *Pnma*, but sometimes nonstandard equivalent space groups *Pbnm* or *Pcmn* are used to describe the structure of $CaTiO_3$) [11,12]. When a perovskite phase of $CdTiO_3$ is cooled down to ~80 K, it undergoes a phase transition to a polar orthorhombic phase with the space group $Pna2_1$ [10].

(1-x)($Na_{0.5}Bi_{0.5}$)TiO_3-$x$$CdTiO_3$ (abbreviated (1-x)NBT-xCdT) solid solution group has not been a popular research object probably due to toxicity of cadmium, which is comparable with toxicity of lead, and low expectations of good ferroelectric properties considering the non-polar nature of $CdTiO_3$ at room temperature.

Interestingly, the solid solutions with $0.4 \leq x \leq 0.6$ are ferroelectric at room temperature. A distinct first order phase transition is revealed by discontinuity in temperature dependence of thermal expansion coefficient [13]. On the other hand, the solid solutions with $0.05 \leq x \leq 0.3$ do not show any signs of a phase transition. They have lower dielectric response and exhibit relaxor properties [13]. The solid solutions with $x \geq 0.7$ are paraelectric at room temperature [13,14], just as $CdTiO_3$.

There have been few attempts to study crystal structure of (1-x)NBT-xCdT solid solutions. Authors in ref. [14] had used the obsolete method to obtain diffraction patterns. Since they had used only pseudocubic

approach, there was no information about possible space groups of these compounds. In our previous study [13], we had presented some information about structural properties of (1-*x*)NBT-*x*CdT solid solutions.

The main purpose of this paper is to further clarify the crystal structure of (1-*x*)NBT-*x*CdT solid solutions. Our analysis is based on polarization measurements, x-ray diffraction, Rietveld analysis and group theoretical considerations.

Materials and Methods

(1-*x*)($Na_{0.5}Bi_{0.5}$)TiO_3-*x*$CdTiO_3$ ((1-*x*)NBT-*x*CdT) ceramics were prepared by solid state reaction from chemical-grade oxides as described in ref. [13]. Samples for dielectric and polarization measurements were prepared in form of 0.5 mm thick ceramic disks with Au electrodes fired at 500˚C. Samples for x-ray diffraction were prepared by crushing the ceramics in pestle and heating obtained powder at 700˚C for 30 minutes, then followed by cooling down to room temperature.

X-ray diffraction patterns were obtained using PANalytical X'Pert PRO diffractometer equipped with multichannel solid-state detector PIXcel. Cu $K\alpha_{1,2}$ radiation was used, the tube was set to 45 kV and 40 mA. Room temperature diffraction patterns were recorded with a step of 0.0131˚ from 10˚ to 150˚ degrees and 77.5 s counting time. Total acquisition time per diffraction pattern was ~1 hour. Anton Paar TTK 450 temperature camera and Anton Paar TCU 100 temperature control unit were used for non-ambient temperature experiments.

Rietveld refinements [15] of obtained powder x-ray diffraction patterns were carried out with BGMN [16] and its graphical user interface Profex [17].

Weak-field dielectric properties in temperature range from −120˚C to 350˚C and frequency region from 100 Hz to 1 MHz were studied using an impedance analyser HP precision LCR meter 4284A with a measuring electric field of 0.4 V/cm. Rate of the temperature change was ~ 2˚C/min. Polarization hysteresis measurements were done using the Sawyer-Tower method in quasistatic limit.

Results and discussion

X-ray diffraction patterns (Fig. 1) indicate that solid solutions (1-*x*)NBT-*x*CdT with $x \geq 0.7$ are isostructural with pure $CdTiO_3$, as it was expected. This is in agreement with completely paraelectric dielectric response (Fig. 2(c)). Rietveld refinements were done in *Pnma* space group. Occupancies of Na^+, Bi^{3+} and Cd^{2+} ions were fixed to corresponding chemical formula solid solutions. An example of fitted diffraction pattern can be seen in Fig. 1. *Pnma* space group is associated with mixed oxygen octahedral tilt system $a^-b^+a^-$ giving rise to both ½(*ooe*) and

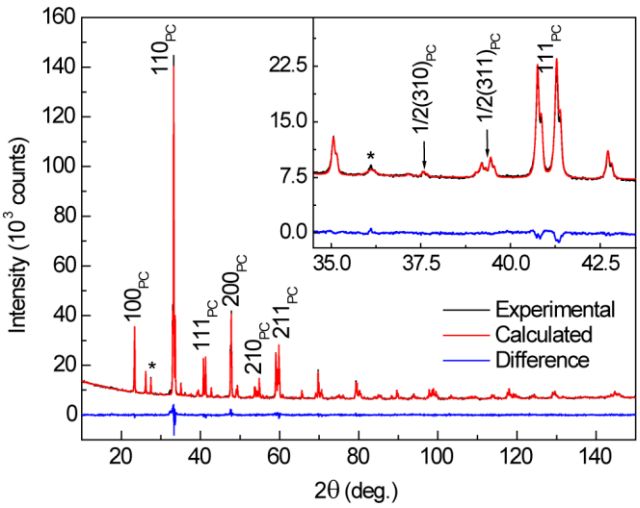

Fig. 1 X-ray diffraction pattern and Rietveld fit with *Pnma* space group of composition 0.2NBT-0.8CdT as a representative of $x \geq 0.7$ solid solutions (the inset represents a magnified fragment of the pattern). Asterisk marks a small TiO_2 impurity. Two superstructure reflections are marked with arrows – $½(310)_{PC}$ corresponding to the in-phase tilting and $½(311)_{PC}$ corresponding to the out-of-phase tilting of the oxygen octahedra. Maxima are indexed according to pseudo-cubic perovskite cell

½(*ooo*) superstructure reflections (where o is odd and e is even Miller index) which are associated with in-phase and out-of-phase octahedral tilting [6]. Additionally there are several superstructure reflections which do not correspond to either of tilting patterns (so called concert reflections). These reflections appear when antiparallel cation shifts are present in the crystalline structure or both of the oxygen octahedral tilting patterns are present. In the case of $CdTiO_3$ and $CaTiO_3$ both conditions are fulfilled [18].

(1-*x*)NBT-*x*CdT solid solutions in the concentration range $0.4 \le x \le 0.6$ are ferroelectric, as it can be seen from polarization hysteresis loops in Fig. 2(d). Also dielectric spectroscopy measurements (Fig. 2(b)) indicate that ferroelectric phase transition occurs at elevated temperatures. The obtained diffraction patterns of these solid solutions are considerably different from those of the compositions with $x \ge 0.7$, as it is shown in Fig. 3 for the composition with $x=0.6$ composition. Superstructure reflections of ½(*ooo*) type and concert reflections cannot be

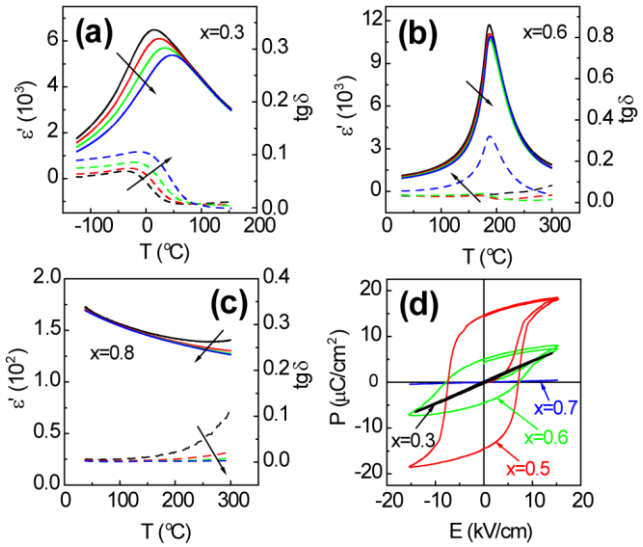

Fig. 2 Temperature-frequency dependences of dielectric permittivity (solid lines) and loss tangent (dashed lines) for (1-*x*)NBT-*x*CdT compositions with $x=0.3$ (a), $x=0.6$ (b) and $x=0.8$ (c), as well as polarization hysteresis loops of (1-*x*)NBT-*x*CdT solid solutions with different $CdTiO_3$ concentrations *x*

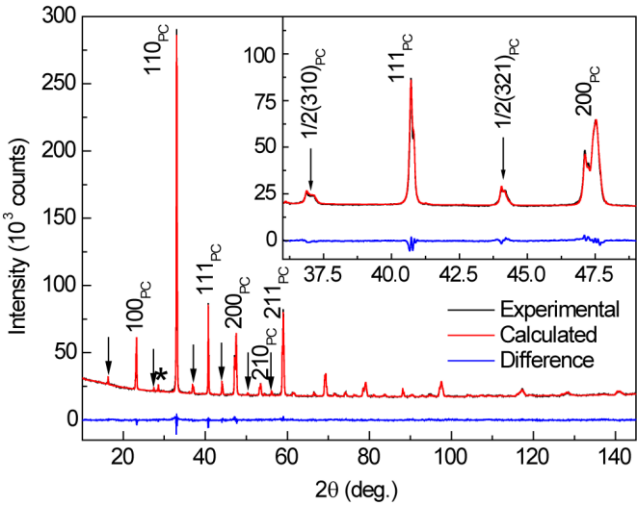

Fig. 3 X-ray diffraction pattern and Rietveld fit with *Imm2* space group of 0.4NBT-0.6CdT composition as a representative of $0.4 \le x \le 0.6$ solid solutions (the inset represents a magnified fragment of the pattern). Asterisk indicates the peak from small TiO_2 impurity, arrows indicate a few superstructure maxima of ½(*ooe*) type. Maxima are indexed according to pseudo-cubic perovskite cell

seen in the diffraction patterns, only strong ½(*ooe*) superstructure reflections are visible, which is a clear sign of an in-phase oxygen octahedral tilt system. Additionally, 111_{PC} is not split, while 200_{PC} reflection is split into three maxima, two of which are not well-separated (see Figs. 4(a) and 4(b)). This is consistent with the orthorhombic symmetry. Such observations point to the $a^+b^+c^+$ octahedral tilting pattern according to Glazer's scheme and the *Immm* space group [19]. This space group cannot be correct, as the studied solid solutions in the $CdTiO_3$ concentration range $0.4 \leq x \leq 0.6$ are ferroelectric (essentially the same diffraction pattern was obtained for both poled and unpoled samples), but *Immm* space group is centrosymmetric. Rietveld calculations for this space group led to a good description of the main perovskite maxima and correct positions of superstructure reflections, while the calculated intensity of superstructure reflections was approximately half as large as the measured intensity. All the above mentioned indicates that the proper space group must be very similar to *Immm*. The group-theoretical analysis performed by Stokes et al [20] extracted a polar space group *Imm2* which is a subgroup of *Immm*. Essentially, in the space group *Imm2* additional atomic displacements along *Z* axis are allowed, unlike in the non-polar supergroup. Initial atomic coordinates for Rietveld refinement were calculated by ISODISTORT tool [21]. Rietveld refinement in this space group gives a very good description of experimental diffraction pattern, as it can be seen in Fig. 3.

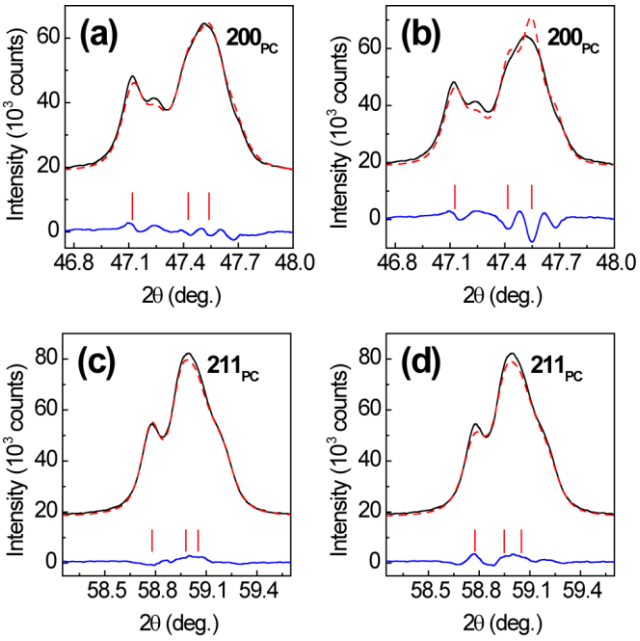

Fig. 4 X-ray diffraction maxima 200_{PC} and 211_{PC} of 0.4NBT-0.6CdT composition. The graphs on the left – (a) and (c) – correspond to calculation results obtained using Rietveld model with anisotropic micro-strains, the graphs on the right – to calculation results obtained using isotropic micro-strain model – (b) and (d); Black solid line corresponds to experimental data, red dashed line – to calculated data, blue solid line – to difference between experimental and calculated data, tick marks indicate positions of Bragg reflections responsible for splitting of the pseudo-cubic maxima

According to ref. [18,22] and our knowledge, $a^+b^+c^+$ octahedral tilt system has never been experimentally detected before. In the *Imm2* space group there are four non-equal A-cation sites. Three of them have distorted square planar environment and one has distorted cubooctahedral coordination (atomic position located at the origin). A proper description of the superstructure reflections is only possible with displacements of the A site cations relative to the surrounding oxygen anions along *Z* axis. Rietveld refinements also show Ti^{4+} off-centring in the oxygen octahedron, which indicates that ferroelectricity arises from both – the A site and the B site ion displacements.

Structural parameters of 0.4NBT-0.6CdT solid solution are summarized in Table 1 and the corresponding model is shown in Fig. 5 [23]. The isotropic Debye-Waller factors (B_{iso}) of the A-site cations were refined as one parameter between all four sites, as it represents more static disorder rather than thermal one. Similarly the isotropic Debye-Waller factors of the oxygen atoms were constrained to one refinement parameter, as it

drastically reduces the number of variables. The low scattering amplitude of oxygen atoms justifies this approach.

Table 1 Structural parameters of 0.4NBT-0.6CdT and 0.7NBT-0.3CdT solid solutions at room temperature

0.4NBT-0.6CdT					
Atoms	Wyckoff pos.	*X*	*Y*	*Z*	B_{iso} (Å^2)
Na/Bi/Cd	a	0	0	0[a]	1.582 (13)
Na/Bi/Cd	a	0	0	0.53633 (85)	
Na/Bi/Cd	b	0	0.5	0.02520 (53)	
Na/Bi/Cd	b	0	0.5	0.49148 (83)	
Ti	e	0.25944 (53)	0.24280 (33)	0.25159 (59)	0.112 (29)
O	e	0.2085 (12)	0.2887 (12)	-0.01245 (74)	1.761 (66)
O	c	0.2806 (12)	0	0.19602 (83)	
O	c	0.2892 (10)	0	0.7567 (25)	
O	d	0	0.77521(99)	0.3257 (11)	
O	d	0	0.7832 (10)	0.7494 (21)	
Space group *Imm2*; *a*=7.64794 (10) Å, *b*= 7.665550 (99) Å, 7.712358 (77) Å R_{wp}=1.31% χ^2=3.40					
0.7NBT-0.3CdT					
Atoms	Wyckoff pos.	*X*	*Y*	*Z*	B_{iso} (Å^2)
Na/Bi/Cd	a	0	0	0	3.126 (19)
Na/Bi/Cd	b	0	0.5	0.5	
Ti	c	0.25	0.25	0.25	0.628 (19)
O	e	0	0.20724 (51)	0.26955 (68)	1.834 (68)
Space group $Im\bar{3}$; *a*=7.711396 (24) R_{wp}=1.52% χ^2=1.81					

[a] *Z* coordinate is fixed to deal with the floating origin in the polar space group.

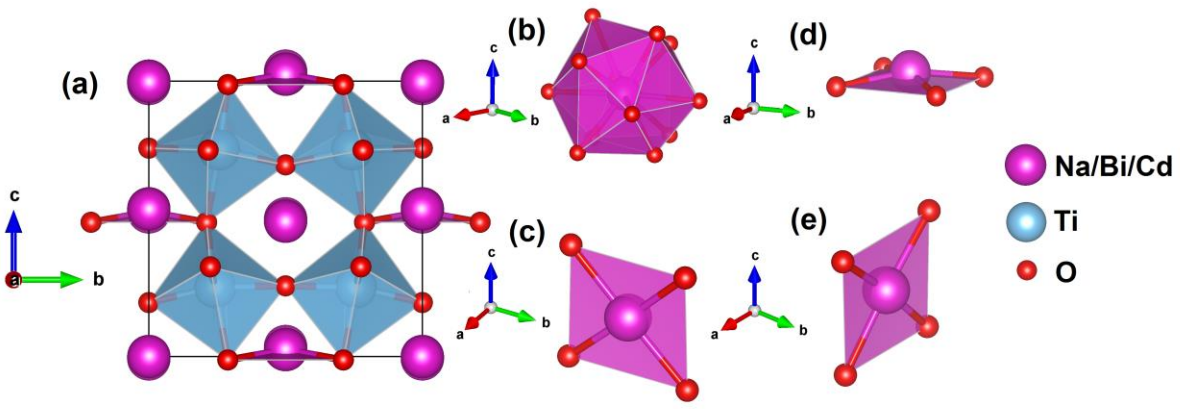

Fig. 5 Structural model of 0.4NBT-0.6CdT solid solution (a) and four nonequal A-site cation positions: (b) Wyckoff position *a* with *Z*=0; (c) Wyckoff position *a* with *Z*=0.53633; (d) Wyckoff position *b* with *Z*=0.02520; (e) Wyckoff position *b* with 0.49148. In each A-site position, cations are shifted along c axis in relation to surrounding oxygen anions, creating a dipole moment

Ferroelectricity in $0.4 \leq x \leq 0.6$ solid solutions arises due to Bi^{3+} ions which condensate unstable polar phonon mode found in the pure $CdTiO_3$ at the Γ point [24]. Interaction of Bi 6*s* with O 2*p* results in set of bonding and antibonding states. Antibonding states can be stabilized by mixing them with empty Bi 6*p* states, but the site symmetry must be such that sp mixing is allowed [25]. In this case, the second order Jahn-Teller distortion leads to a polar structure due to already present polar instability from the $CdTiO_3$ part of the solid solution [25].

Although the A-cation ordering is possible in the *Imm2* space group due to the four non-equal A-cation sites, meaningful results or improved description of diffraction patterns were not obtained assuming several different A-site ordering schemes neither in $x=0.6$ nor in other solid solutions in the studied system. Therefore Rietveld refinement was done as before by fixing atomic occupancies of Na^+, Bi^{3+} and Cd^{2+} ions in every A-site according to chemical formula, which always gives a good fit and meaningful results.

Anisotropic microstrain model was employed for (1-*x*)NBT-*x*CdT solid solutions in the concentration region $0.4 \leq x \leq 0.6$, which gave a better fit to the diffraction patterns (Figs. 4(a) and 4(c)) as compared with traditional isotropic microstrain model (Figs. 4(b) and 4(d)). It must be mentioned that, for the solid solution with $x=0.7$, which undoubtedly has space group *Pnma*, fitting of diffraction pattern is also improved by anisotropic microstrain model, while for the composition with $x=0.8$ it is not. Since the composition with $x=0.7$ is located close to the concentration range where ferroelectric phase exists, the observed anisotropic microstrains can be explained by influence of residual ferroelectric state. The presence of weak maximum in the temperature dependence of dielectric permittivity [13] supports such an assumption.

When the solid solutions in the concentration range $0.4 \leq x \leq 0.6$ are heated, a phase transition from the orthorhombic *Imm2* to the cubic $Im\bar{3}$ space group occurs (accordingly from $a^+b^+c^+$ to $a^+a^+a^+$ oxygen octahedral tilt system). Particular symmetry of the high-temperature phase can be identified by loss of splitting of the 200_{PC} maximum (Fig. 6) and still visible superstructure reflections of ½(*ooe*) type corresponding to the in-phase tilt system. The three non-equivalent distorted square planar sites in *Imm2* (see Fig. 5) transform into one

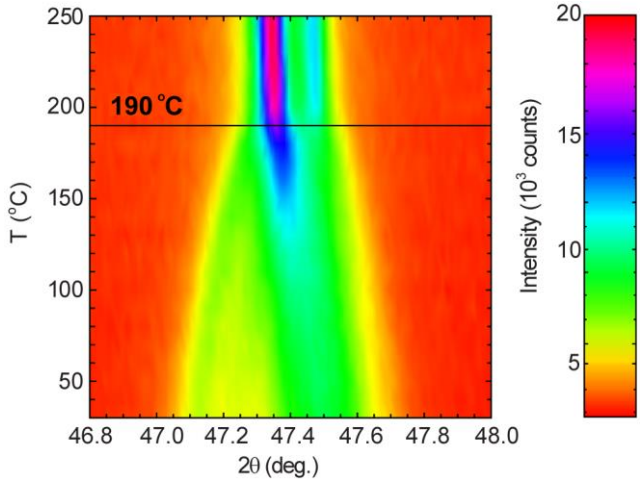

Fig. 6 Contour plot of temperature dependence of 200_{PC} maximum for (1-*x*)NBT-*x*CdT composition with $x=0.6$. Horizontal line at 190˚C indicates phase transition temperature

non-distorted square planar site during the phase transition. The polar distorted cubooctahedrally coordinated A-site in *Imm2* transforms into a nonpolar, but still slightly distorted cubooctahedrally coordinated site characteristic for $Im\bar{3}$ space group [22]. Observed diffraction pattern of the high-temperature phase in the concentration region $0.4 \leq x \leq 0.6$ is analogous to the one in Fig. 7, and refined crystallographic model is equivalent to the one in Fig. 8. The phase transition temperature observed by XRD (Fig. 6) is in a good agreement with the dielectric permittivity measurement data – Fig. 2(b).

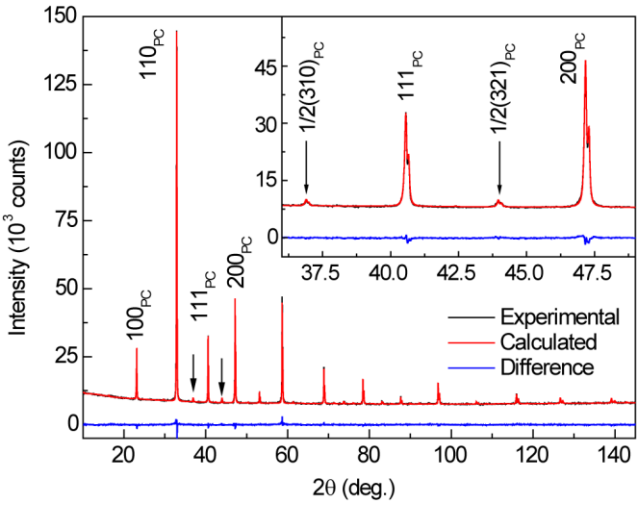

Fig. 7 X-ray diffraction pattern and Rietveld fit with $Im\bar{3}$ space group for (1-*x*)NBT-*x*CdT composition with *x*=0.3 (the inset represents a magnified fragment of the pattern). Arrows indicate some of the visible superstructure reflections

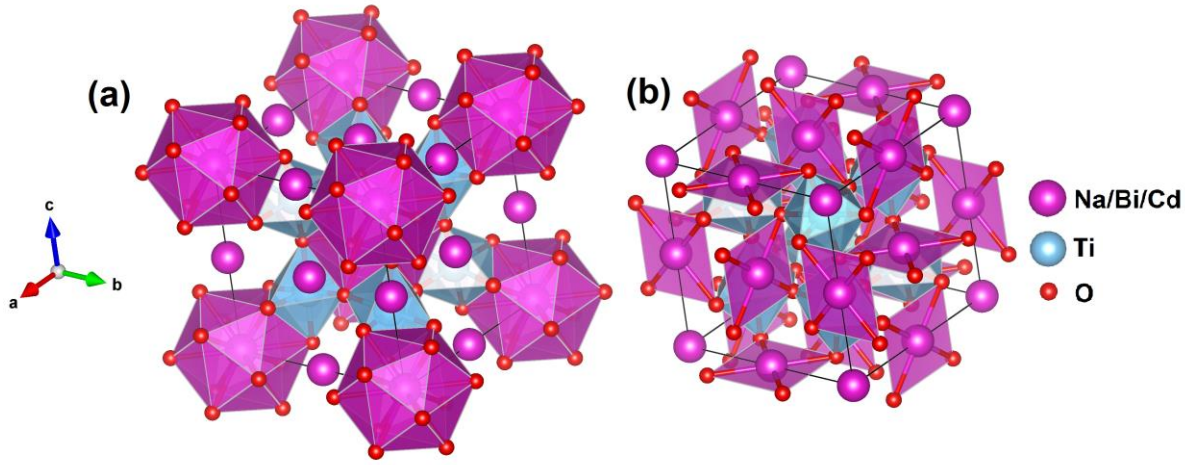

Fig. 8 Structural model of 0.7NBT-0.3CdT solid solution. On the left (a), slightly distorted cubooctahedral coordination sites and, on the right (b), square planar coordination sites are shown

(1-*x*)NBT-*x*CdT solid solutions in the concentration range $0.05 \le x \le 0.3$ are also cubic with the space group $Im\bar{3}$, just as the high-temperature phase in the concentration range $0.4 \le x \le 0.6$. Dielectric spectroscopy in $0.05 \le x \le 0.3$ concentration range shows typical relaxor-ferroelectric dielectric response. Usually perovskite relaxor ferroelectrics have averaged $Pm\bar{3}m$ symmetry [26], which does not have octahedral tilts. But in the solid solutions with $0.05 < x \le 0.3$ we have observed classical relaxor ferroelectric behaviour and a space group with octahedral tilting. Rietveld refinements gave very good fits to both – main perovskite and superstructure maxima (Fig. 7). The crystallographic model created from refined structural parameters (Table 1) can be seen in Fig. 8.

It is evident that Cd^{2+} is responsible for the quite extraordinary square planar coordination in NBT containing solid solutions. Formation of structures with a low coordination number is characteristic feature of closed-shell d^{10} ions and results from *d-s* and *d-s-p* hybrid orbitals [27].

Although $CaTiO_3$ is isostructural with $CdTiO_3$ at room temperature, its solid solutions with NBT behave in a different manner. These solid solutions even with low $CaTiO_3$ concentrations ($x>0.05$) stabilize in the *Pnma* space group [9]. So (1-*x*)NBT-*x*$CaTiO_3$ system does not exhibit any crystal structures not related to one or another component of the solid solution, contrary to (1-*x*)NBT-*x*CdT system. This again emphasizes the fact that the *Pnma* space group is a completely stable form of $CaTiO_3$, but not of $CdTiO_3$ [24].

The unit cell parameters of $Im\bar{3}$, *Imm2* and *Pnma* phases were recalculated to pseudocubic perovskite unit cell parameters a_{PC}, b_{PC} and c_{PC} (Fig. 9) for a simpler comparison. In the $Im\bar{3}$ space group and the *Imm2* space group case recalculation is very easy as their unit cell parameters are equal to doubled pseudocubic unit cell parameters. In case of *Pnma* phase, basing on simple geometric considerations, one can derive pseudocubic unit cell parameters a_{PC}, b_{PC}, c_{PC} and angle β_{PC} from actual orthorhombic lattice parameters (a_{Pnma}, b_{Pnma}, c_{Pnma}):

$$a_{PC} = c_{PC} = \frac{1}{2}\sqrt{a_{Pnma}^2 + c_{Pnma}^2}\ , \tag{1}$$

$$b_{PC} = \frac{1}{2} b_{Pnma}\ , \tag{2}$$

$$\beta_{PC} = \cos^{-1}\left(\frac{a_{Pnma}^2 - c_{Pnma}^2}{a_{Pnma}^2 + c_{Pnma}^2}\right). \tag{3}$$

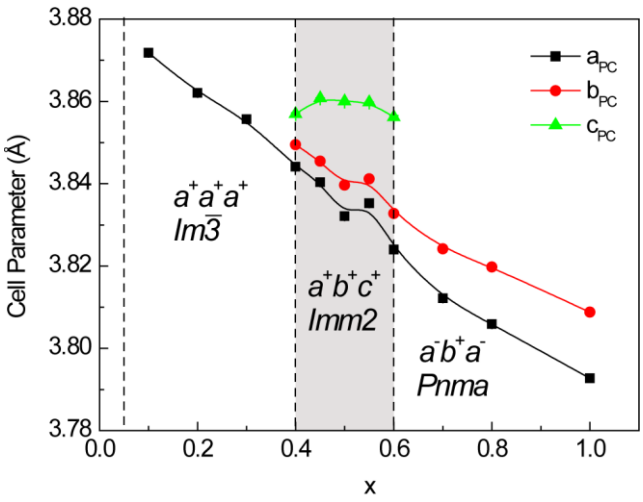

Fig. 9 Pseudocubic unit cell parameters of (1-*x*)NBT-*x*CdT solid solution system. Solid solutions with x≤0.05 resemble pure NBT and the corresponding unit cell parameters are not shown

At very low $CdTiO_3$ concentrations (x≤0.05), x-ray diffraction patterns of (1-*x*)NBT-*x*CdT highly resemble pure NBT, as it is expected.

Conclusions

Oxygen octahedral tilt system $a^+b^+c^+$, which has never been detected earlier, is observed in ferroelectric (1-*x*)NBT- *x*CdT solid solutions in 0.4≤*x*≤0.6 concentration range. Space group *Imm2* corresponding to $a^+b^+c^+$ tilt system is determined by analysing main perovskite and superstructure maxima with Glazer's method, taking into account ferroelectric behaviour of these solid solutions observed in polarization hysteresis loops. Structural phase transition from *Imm2* to $Im\bar{3}$ space group (accordingly from $a^+b^+c^+$ to $a^+a^+a^+$ oxygen octahedral tilt system) is observed for solid solutions in the 0.4≤*x*≤0.6 concentration range. Bi^{3+} induced condensation of the unstable phonon mode at the Γ point is responsible for the stabilization of the ferroelectric phase in this concentration region.

Relaxor ferroelectric solid solutions in the concentration range 0.05≤*x*≤0.3 are found to be in the $Im\bar{3}$ space group. X-ray diffraction patterns at the elevated temperatures (up to 300˚C) of these solid solutions do not show any structural phase transition.

Origins of the square planar coordination in the $Im\bar{3}$ and *Imm2* space groups are connected with presence of the closed shell Cd^{2+} ions in the solid solution.

Acknowledgements

This work has been supported by National Research Program in the framework of project "Multifunctional Materials and composites, photonics and nanotechnology (IMIS2)".

References

[1] Rao BN, Olivi L, Sathe V, Ranjan R (2016) Electric field and temperature dependence of the local structural disorder in the lead-free ferroelectric $Na_{0.5}Bi_{0.5}TiO_3$: An EXAFS study. Phys Rev B 93:024106. doi: 10.1103/PhysRevB.93.024106

[2] Aksel E, Forrester JS, Kowalski B, Jones JL, Thomas PA (2011) Phase transition sequence in sodium bismuth titanate observed using high-resolution x-ray diffraction. Appl Phys Lett 99:222901. doi: 10.1063/1.3664393

[3] Dunce M, Birks E, Antonova M, Plaude A, Ignatans R, Sternberg A (2013) Structure and Dielectric Properties of $Na_{1/2}Bi_{1/2}TiO_3$-$BaTiO_3$ Solid Solutions. Ferroelectrics 447:1–8. doi: 10.1080/00150193.2013.821382

[4] Gorfman S, Thomas PA (2010) Evidence for a non-rhombohedral average structure in the lead-free piezoelectric material $Na_{0.5}Bi_{0.5}TiO_3$. J Appl Crystallogr 43:1409–1414. doi: 10.1107/S002188981003342X

[5] Rao BN, Ranjan R (2012) Electric-field-driven monoclinic-to-rhombohedral transformation in $Na_{1/2}Bi_{1/2}TiO_3$. Phys Rev B 86:134103. doi: 10.1103/PhysRevB.86.134103

[6] Glazer AM (1975) Simple ways of determining perovskite structures. Acta Crystallogr Sect A 31:756–762. doi: 10.1107/S0567739475001635

[7] Jones GO, Thomas PA (2002) Investigation of the structure and phase transitions in the novel A-site substituted distorted perovskite compound $Na_{0.5}Bi_{0.5}TiO_3$. Acta Crystallogr Sect B 58:168–178. doi: 10.1107/S0108768101020845

[8] Dorcet V, Trolliard G, Boullay P (2008) Reinvestigation of phase transitions in $Na_{0.5}Bi_{0.5}TiO_3$ by TEM. Part I: First order rhombohedral to orthorhombic phase transition. Chem Mater 20:5061–5073. doi: 10.1021/cm8004634

[9] Birks E, Dunce M, Ignatans R, Kuzmin A, Plaude A, Antonova M, Kundzins K, Sternberg A (2016) Structure and dielectric properties of $Na_{0.5}Bi_{0.5}TiO_3$-$CaTiO_3$ solid solutions. J Appl Phys 119:074102. doi: 10.1063/1.4942221

[10] Kennedy BJ, Zhou Q, Avdeev M (2011) The ferroelectric phase of $CdTiO_3$: A powder neutron diffraction study. J Solid State Chem 184:2987–2993. doi: 10.1016/j.jssc.2011.08.028

[11] Sasaki S, Prewitt CT, Bass JD, Schulze WA (1987) Orthorhombic perovskite $CaTiO_3$ and $CdTiO_3$: structure and space group. Acta Crystallogr Sect C 43:1668–1674. doi: 10.1107/S0108270187090620

[12] Lufaso MW, Woodward PM (2001) Prediction of the crystal structures of perovskites using the software program SPuDS. Acta Crystallogr Sect B 57:725–738. doi: 10.1107/S0108768101015282

[13] Dunce M, Birks E, Antonova M, Zauls V, Kundzinsh M, Fuith A (2011) Structure and Physical Properties of $Na_{1/2}Bi_{1/2}TiO_3$-$CdTiO_3$ Solid Solutions. Ferroelectrics 417:93–99. doi: 10.1080/00150193.2011.578502

[14] Герцен НП, Лебедев ВМ, Стембер НГ и. др. (1979) Исследование твердых растворов системы $(Na_{0.5}Bi_{0.5})TiO_3$-$CdTiO_3$. Неорг материалы 15:2202–2206.

[15] Rietveld HM (1967) Line profiles of neutron powder-diffraction peaks for structure refinement. Acta Crystallogr 22:151–152. doi: 10.1107/S0365110X67000234

[16] Taut T, Kleeberg R, Bergmann J (1998) The new seifert Rietveld program BGMN and its application to quantitative phase analysis. Mater Struct 5:57–66.

[17] Doebelin N, Kleeberg R (2015) Profex: a graphical user interface for the Rietveld refinement program BGMN. J Appl Crystallogr 48:1573–1580. doi: 10.1107/S1600576715014685

[18] Woodward DI, Reaney IM (2005) Electron diffraction of tilted perovskites. Acta Crystallogr Sect B 61:387–399. doi: 10.1107/S0108768105015521

[19] Glazer AM (1972) The classification of tilted octahedra in perovskites. Acta Crystallogr Sect B 28:3384–3392. doi: 10.1107/S0567740872007976

[20] Stokes HT, Kisi EH, Hatch DM, Howard CJ (2002) Group-theoretical analysis of octahedral tilting in ferroelectric perovskites. Acta Crystallogr Sect B 58:934–938. doi: 10.1107/S0108768102015756

[21] Campbell BJ, Stokes HT, Tanner DE, Hatch DM (2006) ISODISPLACE: A web-based tool for exploring structural distortions. J Appl Crystallogr 39:607–614. doi: 10.1107/S0021889806014075

[22] Woodward PM (1997) Octahedral Tilting in Perovskites. II. Structure Stabilizing Forces. Acta Crystallogr

B 53:44–66. doi: 10.1107/S0108768196012050
[23] Momma K, Izumi F (2011) VESTA 3 for three-dimensional visualization of crystal, volumetric and morphology data. J Appl Crystallogr 44:1272–1276. doi: 10.1107/S0021889811038970
[24] Moriwake H, Kuwabara A, Fisher CAJ, Taniguchi H, Itoh M, Tanaka I (2011) First-principles calculations of lattice dynamics in $CdTiO_3$ and $CaTiO_3$: Phase stability and ferroelectricity. Phys Rev B 84:104114. doi: 10.1103/PhysRevB.84.104114
[25] Benedek NA, Fennie CJ (2013) Why are there so few perovskite ferroelectrics? J Phys Chem C 117:13339–13349. doi: 10.1021/jp402046t
[26] Bokov AA, Ye Z-G (2006) Recent progress in relaxor ferroelectrics with perovskite structure. J Mater Sci 41:31–52. doi: 10.1007/s10853-005-5915-7
[27] Röhler J (1996) On the stereochemistry of cations in the doping block of superconducting copper oxides. J Supercond 9:457–461. doi: 10.1007/BF00727296

Institute of Solid State Physics, University of Latvia as the Center of Excellence has received funding from the European Union's Horizon 2020 Framework Programme H2020-WIDESPREAD-01-2016-2017-TeamingPhase2 under grant agreement No. 739508, project CAMART²

Figure 9

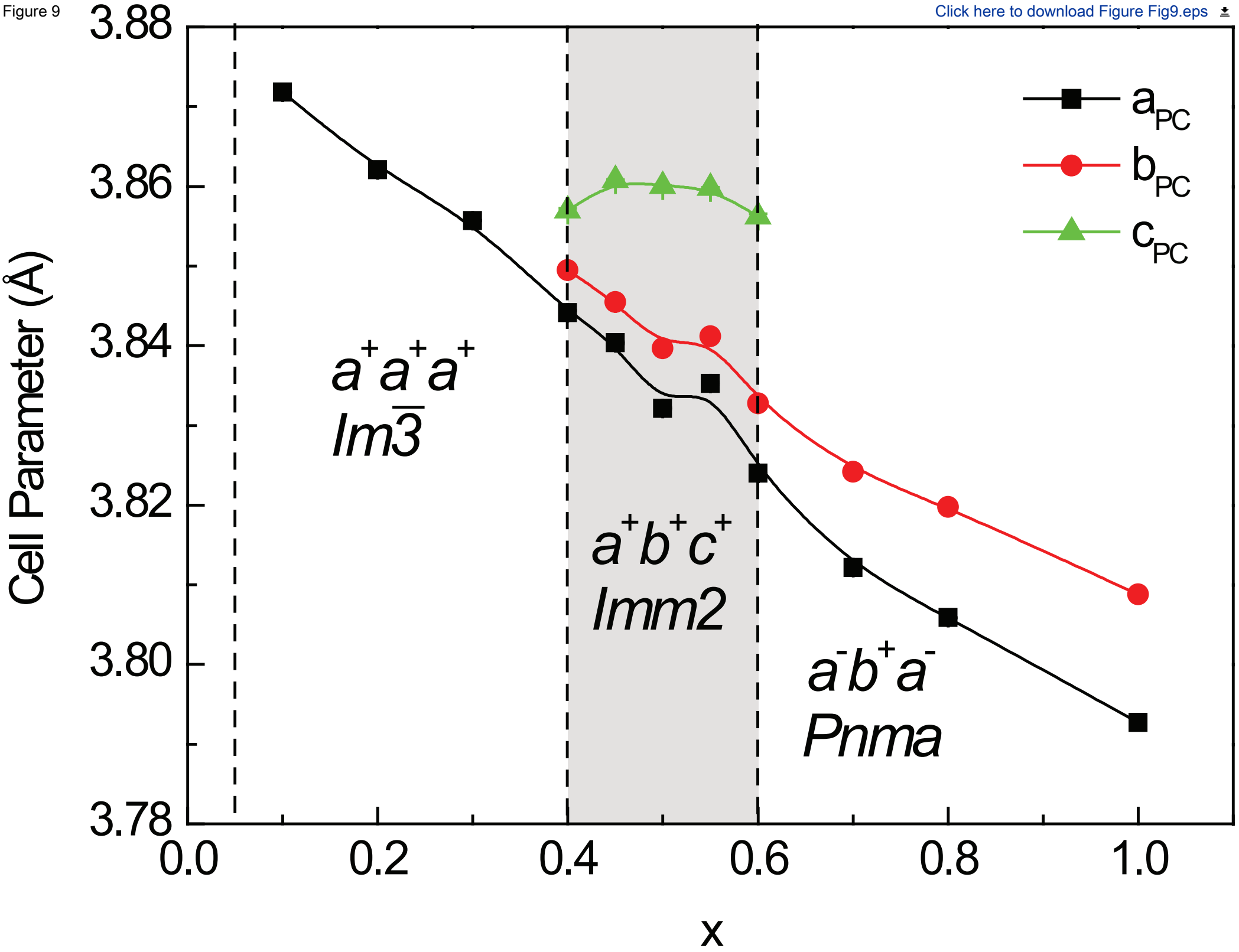

Figure 1

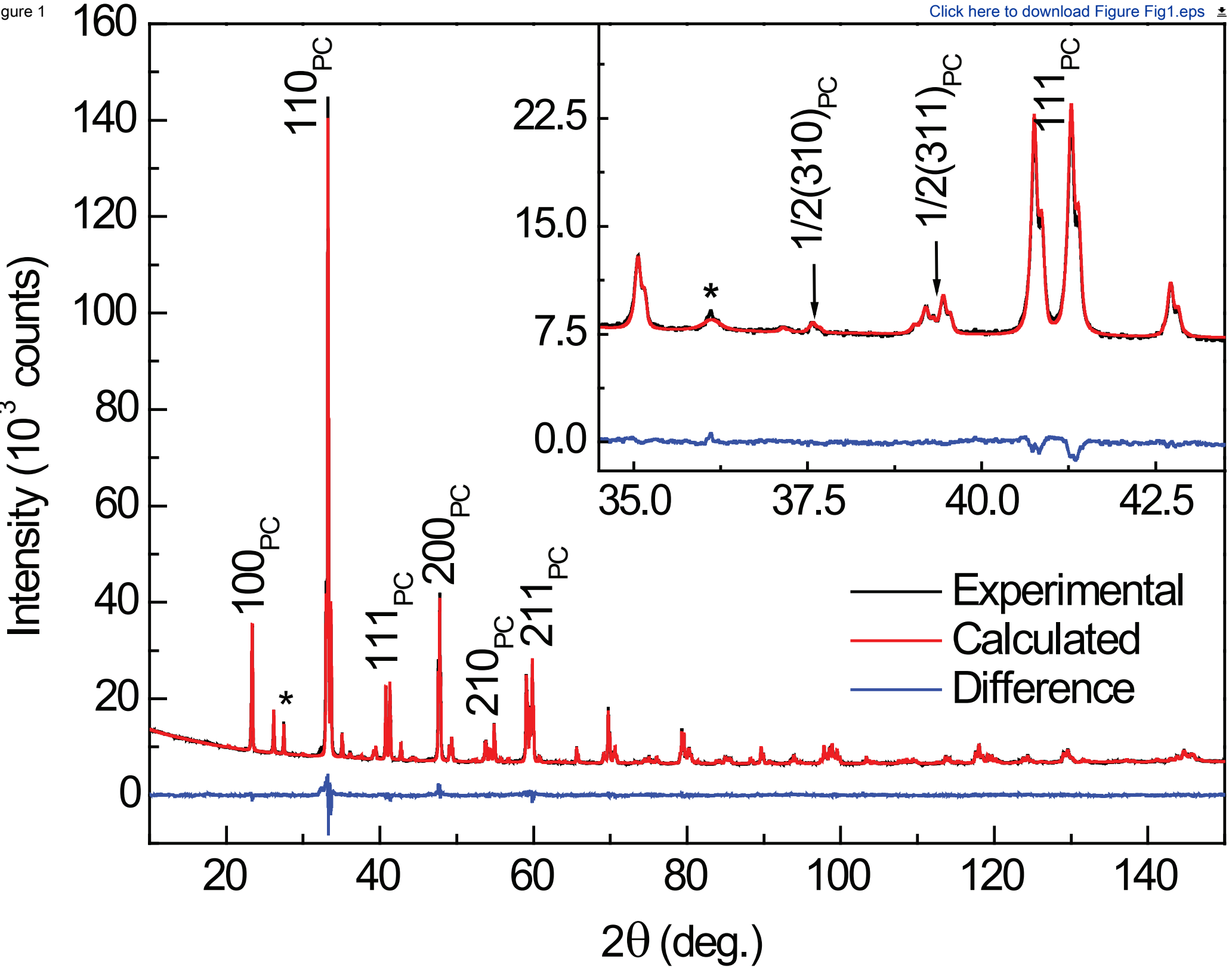

Figure 2

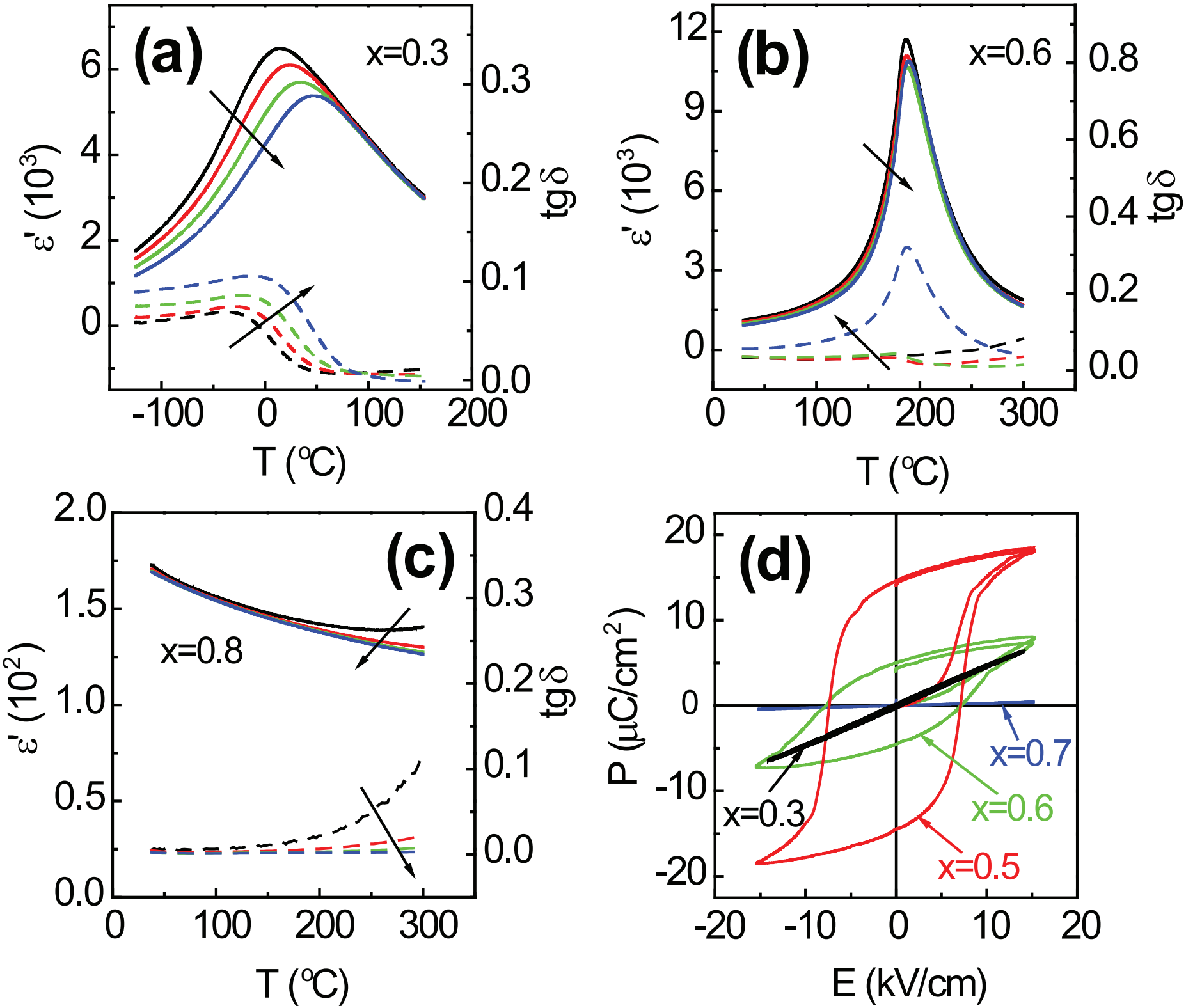

Figure 3

Click here to download Figure Fig3.eps

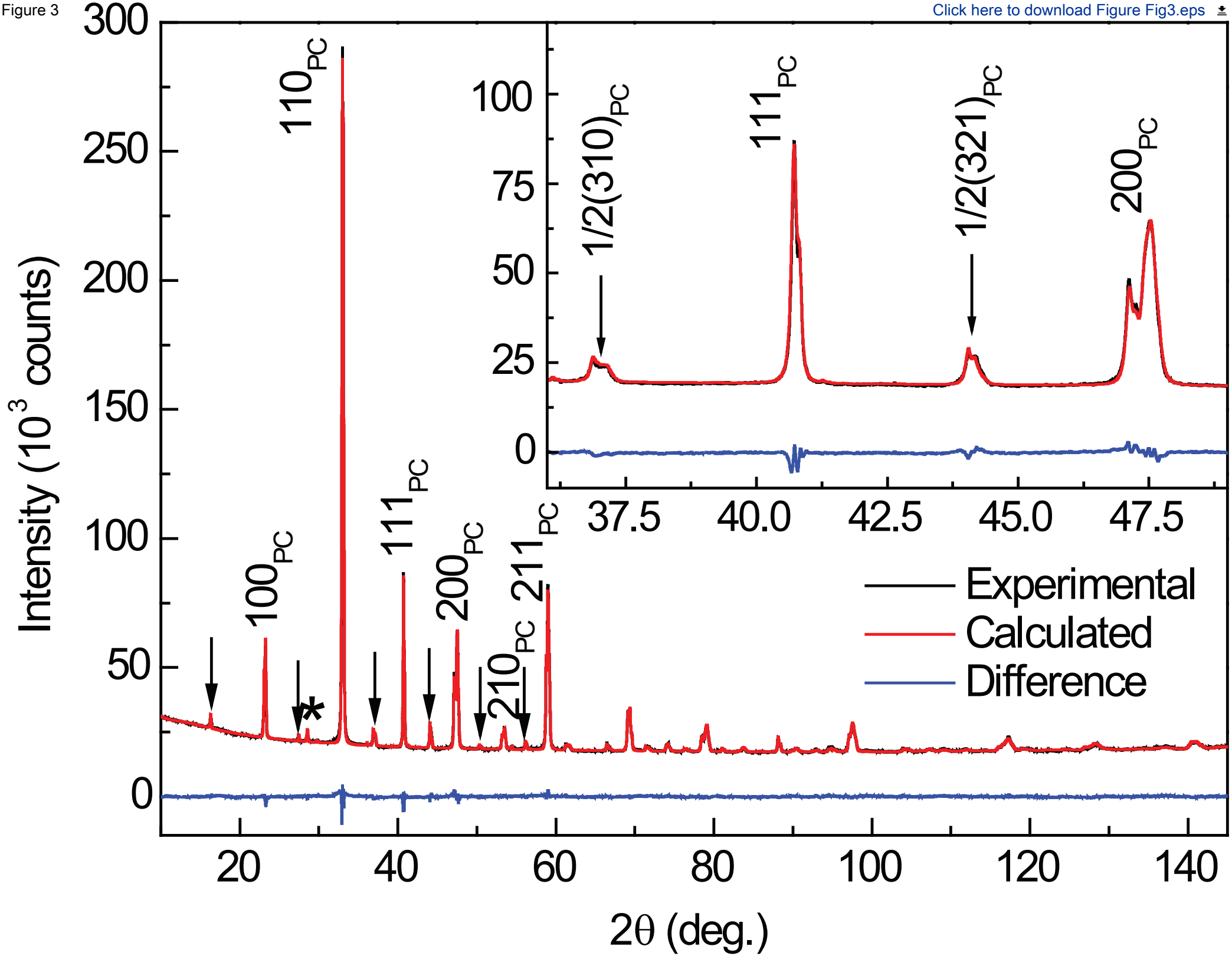

Figure 4

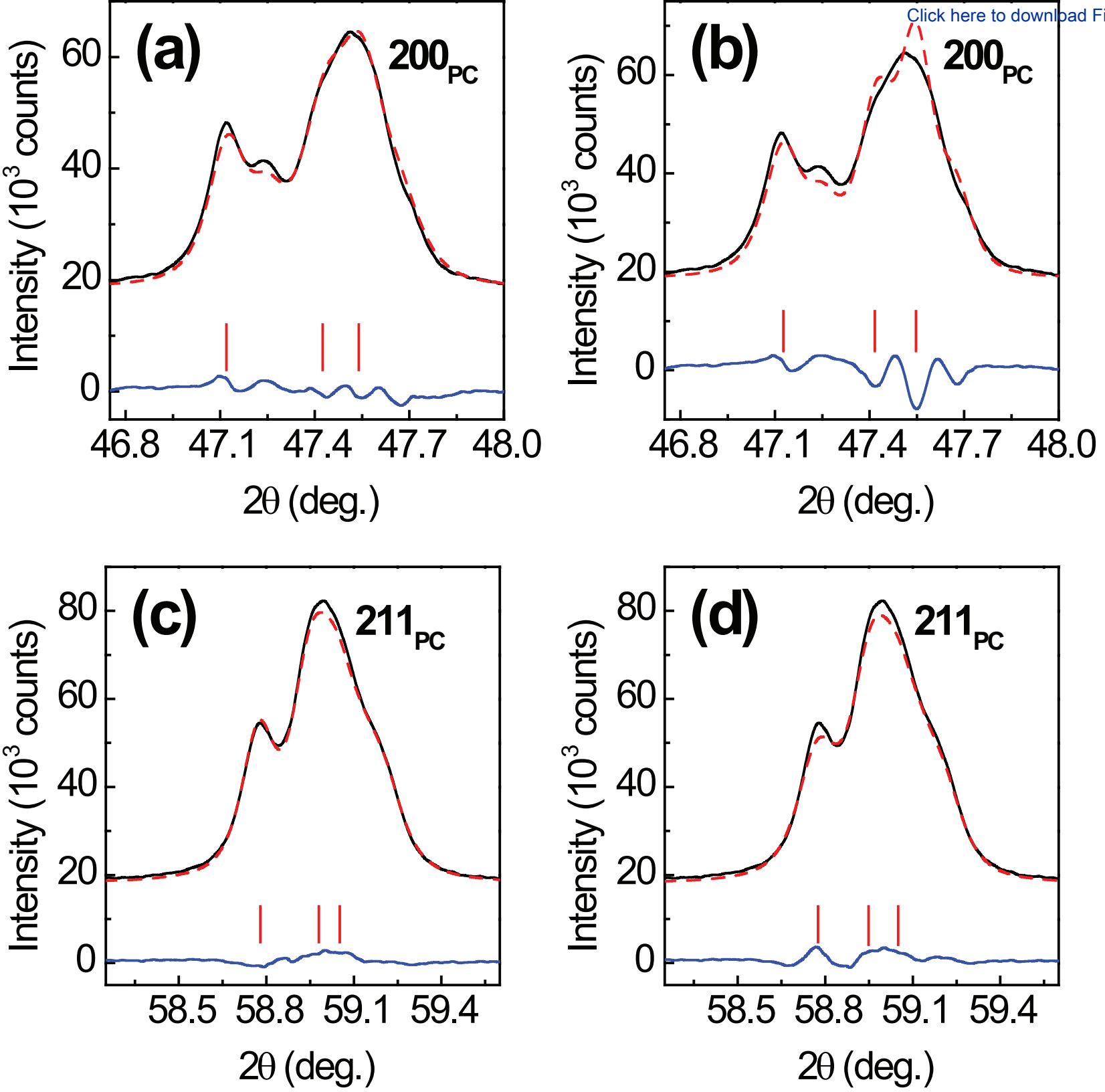

Figure 5

Click here to download Figure Fig5.tif

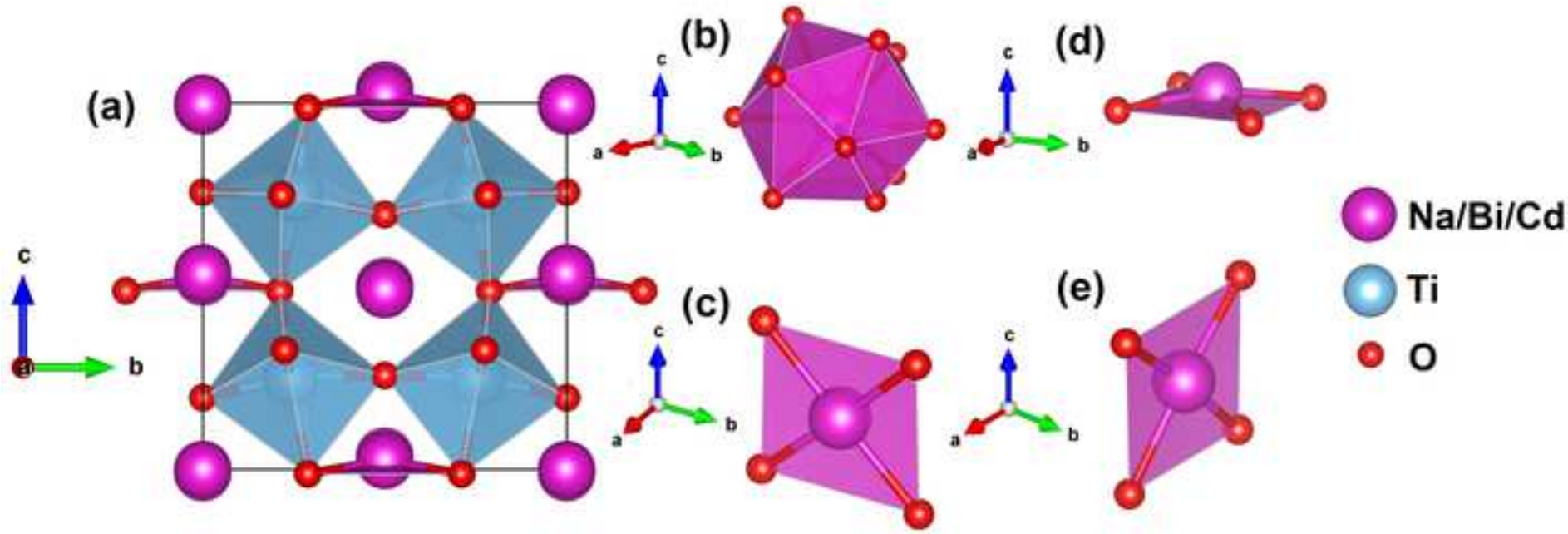

Figure 6

Click here to download Figure Fig6.eps

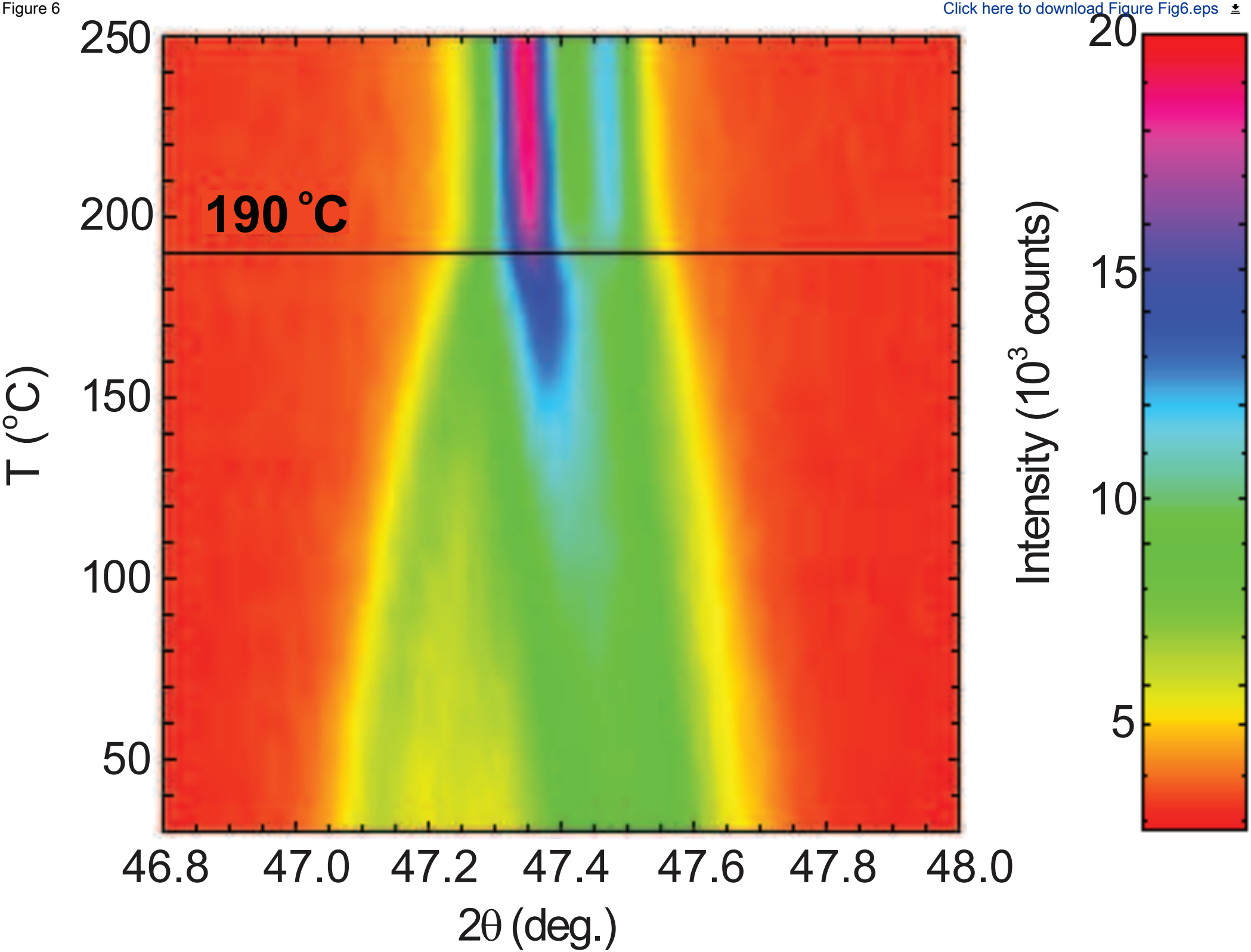

Figure 7

Click here to download Figure Fig7.eps

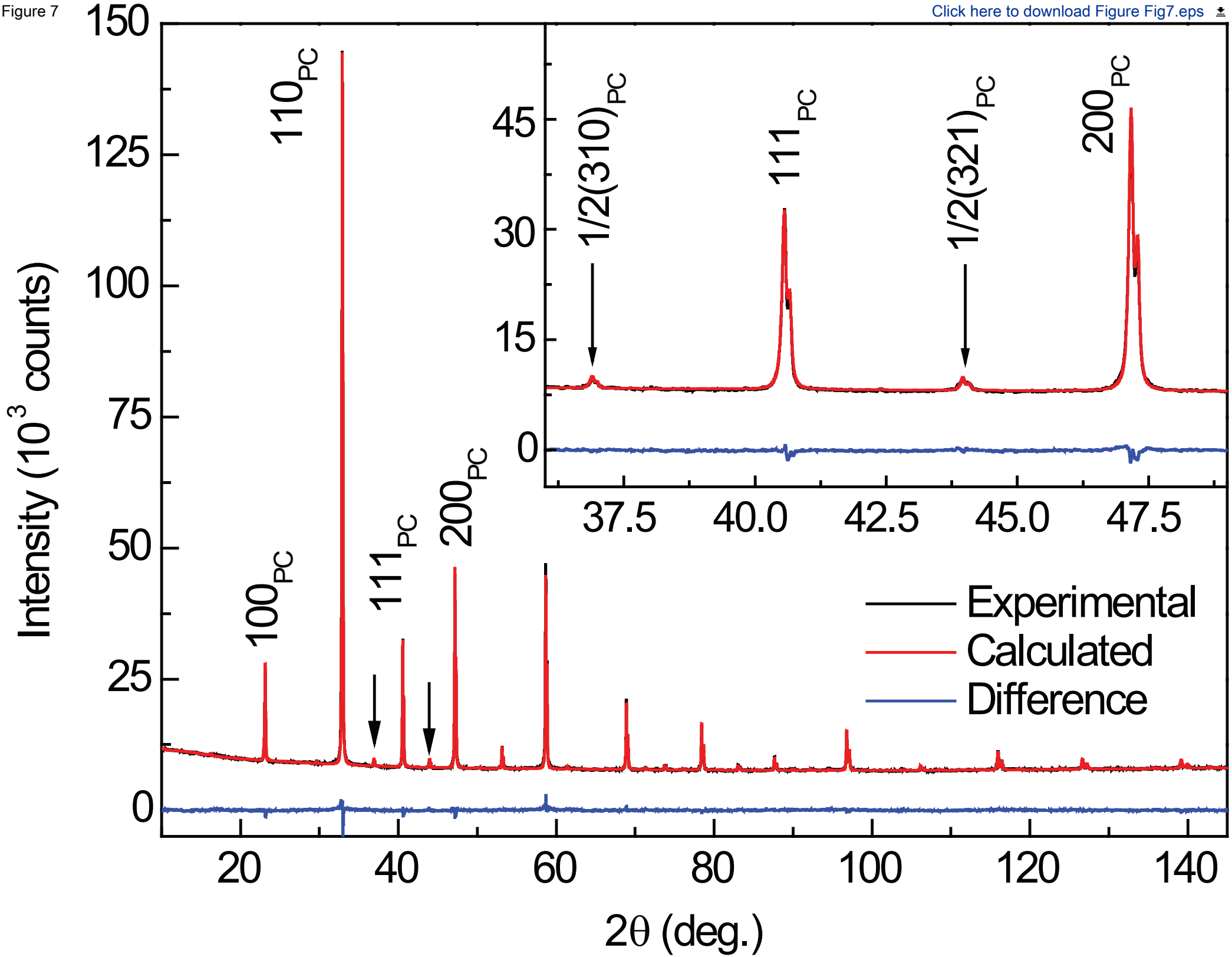

Figure 8

Click here to download Figure Fig8.tif

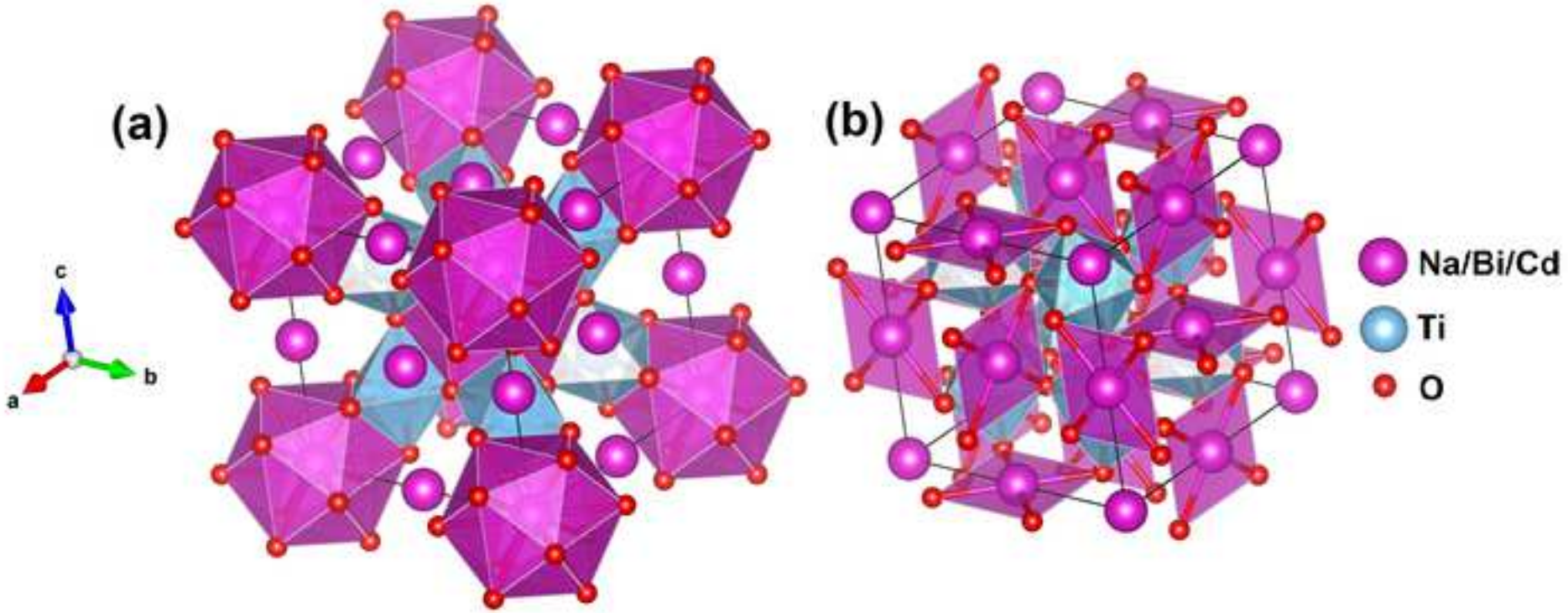

Table 1 Structural parameters of 0.4NBT-0.6CdT and 0.7NBT-0.3CdT solid solutions at room temperature

0.4NBT-0.6CdT					
Atoms	Wyckoff pos.	*X*	*Y*	*Z*	B_{iso} (Å^2)
Na/Bi/Cd	a	0	0	0[a]	1.582 (13)
Na/Bi/Cd	a	0	0	0.53633 (85)	
Na/Bi/Cd	b	0	0.5	0.02520 (53)	
Na/Bi/Cd	b	0	0.5	0.49148 (83)	
Ti	e	0.25944 (53)	0.24280 (33)	0.25159 (59)	0.112 (29)
O	e	0.2085 (12)	0.2887 (12)	-0.01245 (74)	1.761 (66)
O	c	0.2806 (12)	0	0.19602 (83)	
O	c	0.2892 (10)	0	0.7567 (25)	
O	d	0	0.77521(99)	0.3257 (11)	
O	d	0	0.7832 (10)	0.7494 (21)	
Space group *Imm2*; *a*=7.64794 (10) Å, *b*= 7.665550 (99) Å, 7.712358 (77) Å R_{wp}=1.31% χ^2=3.40					
0.7NBT-0.3CdT					
Atoms	Wyckoff pos.	*X*	*Y*	*Z*	B_{iso} (Å^2)
Na/Bi/Cd	a	0	0	0	3.126 (19)
Na/Bi/Cd	b	0	0.5	0.5	
Ti	c	0.25	0.25	0.25	0.628 (19)
O	e	0	0.20724 (51)	0.26955 (68)	1.834 (68)
Space group $Im\bar{3}$; *a*=7.711396 (24) R_{wp}=1.52% χ^2=1.81					

[a] *Z* coordinate is fixed to deal with the floating origin in the polar space group.